Nanomed. J.12(2): 202-215, Spring 2025

RESEARCH PAPER

Fe_3O_4@Poly-dopamine as T_2W MR Nanoprobe for breast cancer detection and as inhibitory Agent in Helicobacter *Pylori*

Mohammad Ghaderian[1], Mohammad Reza Salamat[1*], Daryoush Shahbazi-Gahrouie[1*], Fahimeh Hossien Beigi[2] , Amir Sajedi[3], Gholam Reza Amiri[4], Tahmineh Narimani[5]

[1] Department of Medical Physics, School of Medicine, Isfahan University of Medical Sciences, Isfahan, Iran
[2] Department of Biophysics Falavarjan Branch, Islamic Azad University, Isfahan, Iran
[3]Department of Bacteriology and Virology, School of Medicine, Isfahan University of Medical Sciences, Isfahan, Iran
[4]Falavarjan Branch, Islamic Azad University, Isfahan, Iran
[5]Department of Bacteriology and Virology, Faculty of Medicine, Isfahan University of Medical Sciences, Isfahan, Iran

ABSTRACT

Objective(s): Recently, magnetic nanoparticles coated with different ligands have been utilized in diagnosis, drug delivery, and therapy. This study aimed to synthesize, characterize, and apply Fe_3O_4 coated with Poly Dopamine (PDA) as an MR imaging nanoprobe and its application in metronidazole-resistant helicobacter pylori (H.pylori).

Materials and Methods: Fe_3O_4 nanoparticles were characterized and their cytotoxicity was determined in MCF-7 cell lines. Then, coated and non-coated nanoparticles were injected intravenously into 9 xenograft BALB/C mice, and the signal intensity of the T_2-weighted MR was assessed. Iron concentrations were measured by ICP-AES, and histopathological assessment was done on harvested critical organs. Finally, The standard disk diffusion method was also used to identify the H.pylori resistance to metronidazole. The minimum inhibitory concentrations and the minimum bactericidal concentration of uncoated and coated iron oxide nanoparticles were investigated.

Results: The MTT assay showed low cytotoxicity at 512 µg/ml. T_2 relaxation times of tumors were lower compared to normal tissues. ICP-AES results indicated that the NPs accumulated mostly in the spleen and liver. The histopathology study demonstrated that the vital organ tissues had less morphologic abnormality and apoptotic changes. The minimum inhibitory and minimum bactericidal concentrations of ION@PDA were 16-64 µg/ml and 16-128 µg/ml, respectively.

Conclusion: Due to the high permeability of nanoprobes in tumors, less cytotoxicity, and its inhibitory effects on metronidazole-resistant H.pylori, ION@PDA may be used as a nano contrast agent in MR imaging for the detection of MCF-7 cells.

Keywords: *Magnetic Iron Oxide Nanoparticles, Breast Cancer, Magnetic Resonance Imaging, Helicobacter pylori*

How to cite this article
Ghaderian M, Salamat MR, Shahbazi-Gahrouie D, Hossien Beigi F, Sajedi A, Amiri GhR, Narimani T. Fe_3O_4@Poly-dopamine as T_2W MR Nanoprobe for breast cancer detection and as inhibitory Agent in Helicobacter Pylori. Nanomed J. 2025; 12: 202-215. DOI: 10.22038/nmj.2025.77014.1872

INTRODUCTION

Nanoparticles considered beneficial agents in diagnostic imaging, drug delivery, and treatment [1][2], have piqued the interest of researchers in recent years due to their facilitated synthesis process and high surface-to-volume ratio. They are proven to enhance the durability of the medication in blood circulation, and increase its therapeutic efficacy, targeted delivery, and drug uptake [3, 4], all of which lead to less drug toxicity and diminished related side effects. Nanoparticles smaller than 100 nm have

* *Corresponding authors: Email:salamat@med.mui.ac.ir ; shahbazi@med.mui.ac.ir*
Note. This manuscript was submitted on December 20, 2023; approved on July 21, 2024

demonstrated specialized compatibilities, such as the increased likelihood of rapidly absorbing and transferring drugs, prompt distribution, and successful bonding to biomolecules. The surfaces of magnetic nanoparticles conjugated with tumor-specific biomarkers (nanoprobes) or anti-tumor monoclonal antibodies (mAb) offer a distinct way to detect and localize the cancer lesions [5] while leaving the normal tissues uncompromised [6]. Studies are progressing on developing nanoprobes for treating cancer via different physical and chemical techniques as substitution and integrated therapeutic approaches. These nanoprobes accumulate at the tumor lesion and offer high signal intensity, facilitating the diagnosis with increased contrast between cancerous and normal tissues [7].

Superparamagnetic iron oxide nanoparticles (IONs), including Fe_3O_4, combine the benefits of both imaging and therapy in oncology, and much work has gone into developing them. Various techniques, such as co-precipitation, sonochemical, and green synthesis, have been employed for synthesizing IONs [8]. Their prominent characteristics include plausible size, stability, high permeability, biocompatibility, and lack of toxicity, which can be further improved by adopting a surface modification approach [9]. The size and form of IONs play a crucial role in boosting the efficacy of cancer cell detection and therapy. Moreover, IONs have distinctive features for MR imaging, including non-toxicity, magnetic properties, and biocompatibility. Transverse magnetization vector can be further de-phased by IONs, thus, decreased T_2 and T_2* relaxation times result in hyposignal images, which can offer IONs as a potent negative MRI agent [10].

IONs, as a chemotherapeutic medication, have some drawbacks, including low chemical stability, cellular penetrability, and significant cytotoxicity. Additionally, ION-based tumor therapy falls short in delivering the necessary treatment to the tumor's central region due to its limited vascular system, which leads to cancer recurrence, especially when the hydrodynamic size of nanoparticles is more than 60 nm [11]. Moreover, the reticuloendothelial system rapidly removes these nanoparticles from the vascular system. Some coating substances were employed to alleviate this problem and produce nanoprobe-based IONs, though they have not been fully explored in vivo settings. Numerous biomaterials, including anti-cancer proteins, enzymes, and antibodies, can be conjugated with Fe_3O_4 NPs. For instance, Fe_3O_4 nanoparticles coated with polyacrylic acid (PAA) and modified by 3-amino propanol showed small particle size, good dispersion in water, and enhanced T_1-weighted imaging of tumor sites [12]. Another study reported the synthesis of Fe_3O_4@ZIF-8-Zn–Mn nanoparticles, which demonstrated pH- and glutathione-responsive T_1–T_2 dual-mode contrast effects [13]. Despite the advantages of Fe_3O_4 nanoparticles including low toxicity, relatively low price, and high saturation magnetization, however, they have limitations such as the potential for magnetic interference with other ions and the need for specific coatings to improve stability and biocompatibility [14].

Poly Dopamine (PDA) is a nature-based bio-polymer material with considerable features and strong tissue adhesion, which was used as a ubiquitous coating material for IONs, namely the exterior of Fe_3O_4 [15]. PDA is a molecule with a positive charge at low pH, strongly conjugated to molecules with a negative charge with high permeability [16]. Additionally, PDA has a sufficient interfacial consistency, which can coat nanoparticles and contribute to enhanced hyper-signal MR images with high contrast.

Magnetic resonance imaging can be considered a legitimate noninvasive method for early cancer diagnosis [17]. Drug delivery imaging is a technique that employs both the loading of nanomagnetic-based probes with particular conjugation and guiding these probes to the desired target utilizing external magnetic fields [5]. Human epidermal growth factor receptor-2 (HER-2) can be seen in 25-30 percent of patients suffering from breast cancer. This receptor demonstrates a target point for the nanoparticle in medications. Breast cancer cells expressing HER2 are reportedly more aggressive; as a result, detecting HER2-positive breast cancer in its initial phases can considerably boost the survival rate of the suffering patients. The intracellular kinase domain of the HER2 gene encodes a transmembrane receptor protein (an extracellular ligand-bind domain) with tyrosine kinase activity; in conjunction with iron oxide NPs, the PDA coating functions as a significant contrast agent in MR imaging [18]. PDA-coated Fe_3O_4 nanoparticles (ION-PD) were produced, and their MR imaging contrast agent capabilities were examined. To the authors' knowledge, no published work has evaluated the cytotoxicity and in vivo setting of ION-PD as an MRI agent in breast cancer cells (MCF-7).

H.pylori is a spiral-shaped gram-negative bacterium responsible for causing peptic ulcer diseases and various gastric malignancies worldwide [19, 20]. However, the effectiveness of current treatment methods is compromised due to the emergence of antibiotic resistance [21, 22]. Researchers have explored the potential of using iron oxide nanoparticles coated with poly-dopamine to address this issue. These nanoparticles have shown promise due to their

biocompatibility and antibacterial properties. This study aimed to investigate the effects of iron oxide nanoparticles and the antibiotic metronidazole, administered at sub-minimum inhibitory concentration (sub-MIC), in clinical strains of *H.pylori* that are resistant to metronidazole, as well as its potential as a nano contrast agent for MR imaging in MCF-7 cells induced BALB-C mice.

MATERIALS AND METHODS

Materials

NaOH, FeCl3, and FeCl2 were obtained from Merck Company (Kenilworth, New Jersey, USA). Human breast cancer (MCF-7) cells were purchased from (Razi Institute, Isfahan, Iran). They were then cultured in Dulbecco's Modified Eagle's Medium (DMEM)/High Glucose supplemented with 10 percent Fetal Bovine Serum, 1 percent penicillin-streptomycin, and 5 percent CO2 and water-saturated air. Phosphate-buffered saline (PBS) solution, 3-(4,5-dimethylthiazol-2-yl)-2,5 diphenyl tetrazolium bromide (MTT), and dimethyl sulfoxide (DMSO), DMEM was provided by (Sigma-Aldrich, Burlington, MA, USA). The penicillin-streptomycin was prepared from (Thermo Fisher Scientific Ltd., Waltham, Massachusetts, USA) supplied.

Experimental process

Fig. 1 shows a schematic of the procedure of the experiment. Fe_3O_4 nanoparticles were synthesized using the co-precipitation approach previously published methods [23]. Briefly, the formulation of synthesis is as follows:

$$8NaOH + 2FeCl_3 + FeSO_4.(7H_2O)$$
$$Fe_3O_4 + 6NaCl + Na_2SO_4 + 4H_2O + 7H_2O$$

This equation prepared NaOH, $FeCl_3$, and $FeCl_2$ with 0.01, 0.02, and 0.08 molarity, respectively. Then, they were poured simultaneously and boiled in distilled deionized water. The outcome solution was washed and centrifuged to omit any impurities.

ION-PD was synthesized by combining 80 mg of Fe_3O_4 nanoparticles with 80 mg of dopamine hydrochloride (Sigma, Aldrich, Burlington, MA, United States) and 40 ml Tris Base buffer (pH 8.5). It was shaken for 24 hours at room temperature. The NPs were then rinsed numerous times with deionized water and methanol.

Characterization

Since different methods cause different crystallite sizes, unlike particle size, X-ray powder diffraction (XRD) is used to characterize the physiochemical properties of the Fe_3O_4 nanoparticle samples and their crystal structure, according to the Debye Scherrer formula, as follows [24, 25]:

$$d = \frac{0.9 \times \lambda}{B \times COS\Theta}$$

$$d = \frac{0.9 \times 1.789}{1.5 \times \frac{2\Pi}{360} \times cos21} = 73.621\ A^0 = 7.36\ nm$$

Where d is nanoparticles crystalline size; is wavelength and is full width at half maximum.

All nanoparticle characterization features such as the size distribution of the synthesized NPs were obtained by transmission electron microscopy (TEM), the optical absorption spectra of the NPs dispersed in water were recorded using the UV–visible spectrophotometer, and the accuracy coating of PDA to iron oxide was measured by Fourier Transform Infrared (FTIR) spectroscopy were reported by the authors in published papers previously [10, 23, 24].

Cell Culture and Cytotoxicity Assay

The viability of MCF-7 cancer cells was assessed using a standardized MTT assay [26]. To determine the cytotoxicity of ION and ION-PD on the MCF-7 breast cancer cell line, an MTT assay was done. Various doses of ION and ION-PD (32, 64, 128, 256, and 512 µg Fe/ml) were subjected to the cells following 24, 48, and 72 h incubation. In a 96-well plate, 1.5104 cells per well were seeded and incubated for 24, 48, and 72 h at 37°C in DMEM high glucose medium (%5 CO_2). The cells were then cultured in 200 ml media with ION and ION-PD at varying doses and incubation periods. At 24, 48, and 72 h, MTT assays were performed with IONs at 32, 64, 128, 256, and 512 µg/ml levels. The cells were then treated with ION-PD, and MTT assays were performed at 24, 48, and 72 h at doses of 64, 128, 256, and 512 µg/ml. To determine cell viability, the absorbance of each well was quantified at 630 nm with an ELISA reader (Stat Fax 2100, Awareness Tech., Palm City, Florida, USA).

Animals

BALB/C mice (age: 6-7 weeks; average weight: 20 g) were used in this experiment. They were procured from the Jahad Daneshgahi Institute (Isfahan, Iran). They were kept in an isolated animal housing with controlled humidity and temperature at the School of Medicine, Isfahan University of Medical Sciences, in compliance with the Guide for the Care and Use of Laboratory Animals [27]. The Institutional Animal Care and Ethics Committee of Isfahan University of Medical Sciences authorized the mouse study by the ethical

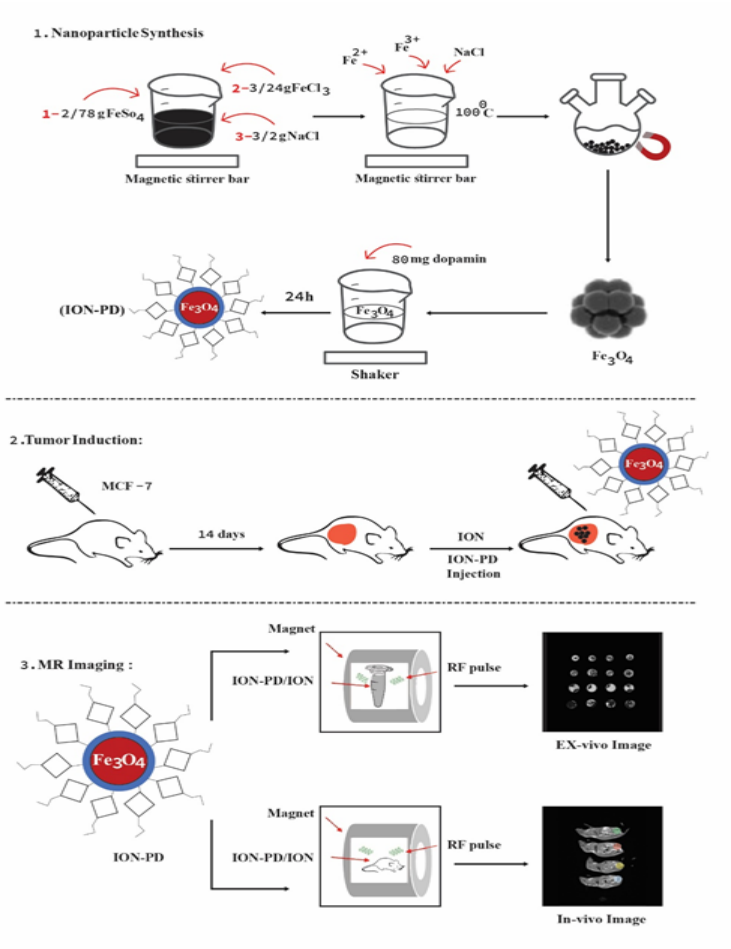

Fig. 1. Schematic steps (1, 2, 3) of the study.

code of IR.MUI.MED.REC.1400.236 and and IR.ARI.MUI.REC.1400.063. They were randomly sorted into three groups (Control, ION, ION-PD) and were given daily sterilized normal mouse food and water. To induce cancer in the mice, all of them were administered with 100 ml MCF-7 cancer cells diluted with PBS into their lower right flank of breast tissue. The tumor lesions were observable after two weeks post-injection with 5-6 mm width (mean weight of tumors: 250 mg). Three weeks into the tumor implantation, the ION and ION-PD group received an intravenous injection of 0.5 mg Fe/kg body weight of the corresponding agent. To do so, the ION and ION-PD were dissolved in deionized water to the injection level of 100 ml. The ION group was injected with 128 µg/ml of ION, while the ION-PD group was administered 256 µg/ml of ION-PD. One cancer-induced mouse was chosen as a control group with no ION or ION-PD injection.

MR imaging

MRI exams were conducted at 12 and 48 hours following ION-PD administration. The mice were sedated with 100 mg/kg of xylazine and ketamine, and a 1.5 T MRI equipment was used to examine them (Siemens ARENA, Munich, Germany). Using the multi spin-echo pulse sequence, T_2-weighted images were acquired with the following parameters: TE = 24, 36, 48, and 60 ms, TR = 3000 ms, slice thickness = 3.5 mm; FA = 150°; FOV = 2.5×2.5 mm; and matrix size = 256×256.

Inductively coupled plasma atomic emission spectroscopy measurements

Inductively coupled plasma atomic emission spectroscopy (ICP-AES) is an agent bio-distribution indicator test equipment (Perkin Elmer Optima 7300 DV type, Waltham, Massachusetts, USA). Mice were euthanized with ketamine (Dublin, OH, USA) 12 and 48 hours post-injection. Consequently, their essential organs were

harvested, including the liver, kidney, spleen, and tumor. They were subjected to an ICP-AES test after the acid digestion. Based on the published literature, the acid digestion technique was used [28]. In brief, a 50-100 mg tissue sample was put in a polyethylene vial, 0.3 ml of %70 perchloric acid was cautiously poured, and the components were thoroughly mixed. After adding 0.6 ml of %28 hydrogen peroxide, the sterile vial jars were kept in the shaking bath for 1 h at room temperature. Then the stock solution was diluted to 2 ml with distilled water, and the contents of the glass vials were leached using a 0.45 mm membrane filter to become clear and colorless. Finally, the samples were analyzed using ICP-AES.

Histopathologic tissue study

To assess the histopathologic features of vital organs, the harvested tissues were fixed in a 10-percent formalin solution and immunostained using hematoxylin and eosin. Then, the images were taken using a ×40 magnified microscope (Amscope7X-45X, Irvine, California, USA).

Bacterial study design

Study design

The study design involved a cross-sectional approach, and patients visiting the endoscopy department of Al-Zahra Hospital in Isfahan, Iran, were included. A total of 110 gastric biopsy samples were collected.

Patients and specimens

The patients included in the study had clinical symptoms of gastrointestinal disorders and had not received prior antibiotics for *H.pylori* infection in the two weeks preceding the study. Two pieces of antral gastric tissue were obtained from each patient, one used for rapid urease testing and the other placed in sterile tubes containing brain heart infusion (BHI) broth supplemented with glucose. These samples were then sent to the microbiology laboratory for further processing. The study included 66 women aged 18-70 years (average age: 53) and 44 men aged 15-48 years (average age: 39) [29, 30].

Bacteria strain and culture conditions

The biopsies were completely crushed between two sterile slides, and the extract obtained was grown in 3% (w/v) Columbia blood agar base (Oxoid, UK) mixed with 1.2% (w/ v) BHI (Oxoid, UK) containing 7% (v/v) sheep blood, 10 mg/mL vancomycin, 10 mg/mL amphotericin, 2500 U/L polymyxin B sulfate salt, 5 mg/mL trimethoprim, 10 mg/mL nalidixic acid (all purchased from Sigma, USA), under microaerophilic conditions (5%~6% O2, 8%~10% CO2, 85% N2) at 37 C for 5 days.

Determining antibiotic sensitivity (Disc diffusion)

A modified disc diffusion method was employed to determine the antibiotic sensitivity of the *H.pylori* isolates. Bacterial suspensions were prepared, streaked onto Müller-Hinton agar supplemented with sheep blood, and incubated with antibiotic discs in a microaerophilic environment at 37°C for 3-7 days. The susceptibility testing and interpretive criteria were based on CLSI guidelines, with an inhibition zone of ≥16 mm indicating sensitivity to metronidazole. In the test mentioned, a standard strain 26695 of *H.pylori* was used as a control [31].

Minimum Inhibitory Concentration (MIC)

Antibacterial properties of Fe_3O_4 nanoparticles and Fe_3O_4@PD AND metronidazole were evaluated using the broth microdilution method to determine the minimum inhibitory concentration (MIC) against bacteria grown in laboratory conditions. To achieve this goal, Brucella broth with 10% fetal bovine serum was added to each well of the 96-well microtiter plate along with different concentrations of antimicrobial substances under our investigation. Then, *H.pylori* was added to each well with a final volume concentration of 5x10^5 CFU/ml, and the plates were incubated for six days in a microaerobic atmosphere at 37 °C. The MIC was determined as the lowest antibiotic concentration inhibiting the visible.

Minimum Bactericidal Concentration (MBC)

To measure the minimum bactericidal concentration, we culture 100 microliters of the suspension from the wells of the upper MICs on Columbia blood agar medium for 5 days in microaerophilic conditions and at 37 degrees. The MBC was the lowest concentration, killing ≥99.9% of the original inoculum. All tests were performed in duplicate.

Statistical analysis

All statistical tests were conducted using IBM SPSS (IBM Corp. Released 2019. IBM SPSS Statistics for Windows, Version 26.0. Armonk, NY: IBM Corp, USA). Mann-Whitney tests were used to compare the means of two independent groups with non-normal distributions. One-way ANOVA was also utilized to see if the ION and ION-PD were responsible for any substantial cytotoxicity. The threshold for statistical significance was set at P = 0.05.

RESULTS

Characterization

The XRD peaks of the ION size are shown in Fig. 2 with the recorded peaks of 575 nm for ION and

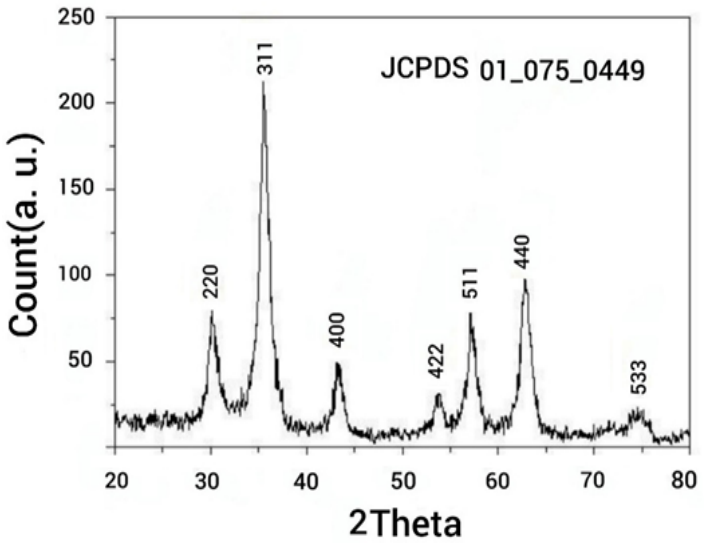

Fig. 2. X-ray diffraction ION (X-ray Tube Anode: Co, Wavelength: 1.7890ºA (Co Kα) Filter.

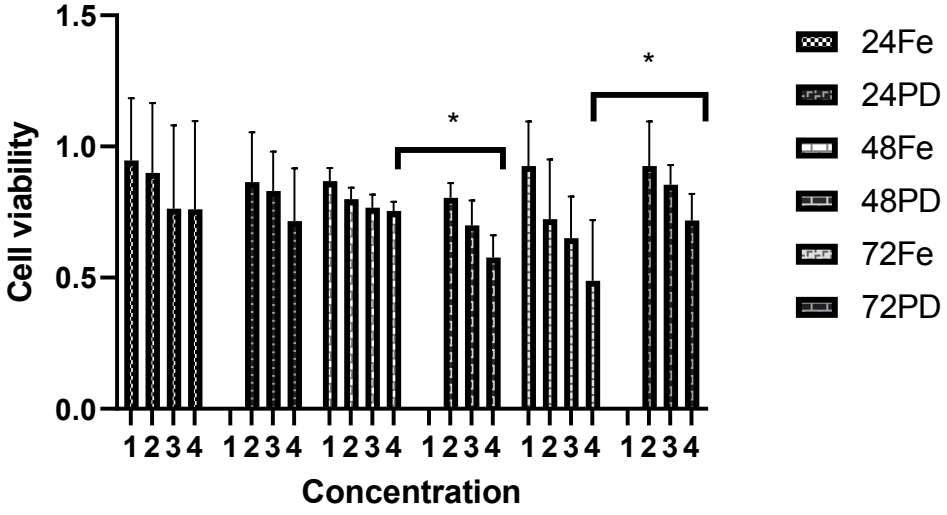

Fig. 3. Cell viability of MCF-7 exposed to different levels of ION and ION-PD in 24, 48, and 72 h of incubation.

539, 1634, 2080, and 3435 nm for ION-PD, based on our previous studies [23] [24].

Authors previously reported the distribution and structural morphology of the ION@PD by TEM, showing a size of 15-20 mm [10, 23]. UV-visible spectrophotometer was also used for evaluating the ION@Pd's optical absorption spectra in MilliQ water [10, 23, 24]. To confirm the integrity of the coating, FTIR was conducted on the ION@PD [10, 32], and it demonstrates two absorption peaks at roughly 1600 and 3500, which can correspond to the coating overlapping.

In vitro cytotoxicity

In terms of cytotoxicity, ION-PD exhibited lower cytotoxicity than ION, with a large margin. The cell viability of MCF-7, with a threshold of %80, is depicted in Fig. 3. Based on the findings, the maximum cytotoxicity of ION was identified at 256 μg/ml in 24 h incubation time with a survival chance of %79, while ION-PD exhibited lower cytotoxicity at 512 μg/ml in the same period. However, the concentrations of 128 μg/ml and 256 μg/ml were considered cytotoxic both in 48 h and 72 h incubation time for ION and ION-PD, respectively. The overall cell viability decreased as

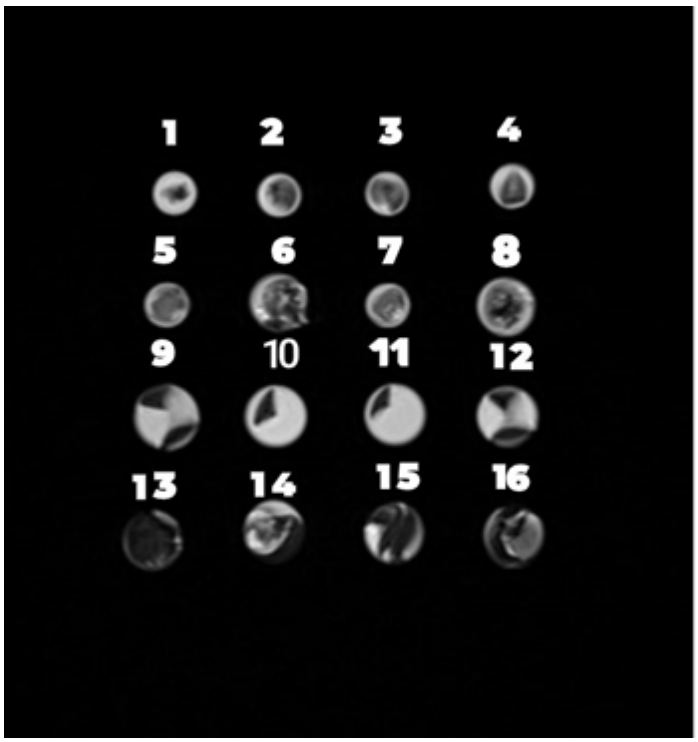

Fig. 4. Ex vivo T2W MR images of organs
1: 48 h ION-PD kidney, 2: 48 h ION kidney, 3: 12 h ION-PD kidney, 4: 12 h ION kidney, 5: 48 h ION-PD tumor, 6: 48 h ION tumor,7: 12 h ION-PD tumor, 8: 12 h ION tumor, 9:48 h ION-PD spleen, 10: 48 h ION spleen, 11: 12 h ION-PD spleen, 12: 12 h ION spleen, 13: 48 h ION-PD liver, 14: 48 h ION liver, 15: 12 h ION-PD liver, 16: 12 h ION liver.

the incubation time increased in ION and ION-PD. The general cell viability ranged between %60 and %95 for all concentrations and incubation times. In the lower concentrations, the cell's viability was stable as the incubation time increased, which can be explained by the mitosis cell-division cycle not hindered by the cytotoxicity of ION and ION-PD. Finally, the concentrations with the least cytotoxicity were chosen for in-vivo studies, 256 and 128 µg Fe/ml for ION-PD and ION, respectively. The optimum concentration of 256 µg/ml was employed for further experimental procedures such as in vitro, ex vivo, and nanoparticle biodistribution assessments

Ex vivo MR imaging

Sensitive organs such as the liver, spleen, kidney, and tumor were chosen to distinguish the efficacy of ION-PD as a negative contrast agent in ex vivo T_2W MR imaging. 12 h and 48 h post-injection mice were sacrificed, the beforementioned organs were harvested, and an MR exam was conducted. As Fig. 4 suggested, injecting ION and ION-PD lowered the signal intensity of tumors and other critical organs, showing the meaningful accumulation of ION and ION-PD in these organs. The aggregation of ION and ION-PD in the organs of 48 h post-injection mice was significantly higher compared to 12 h post-injection mice. Notably, the signal intensity reduction in the ION-PD group was higher than in the ION group, making it a reliable contrast agent in T_2 images.

In vivo MRI

The signal intensity of ION and ION-PD as negative contrast agents were evaluated using an MRI exam. Cancerous and control mice were first anesthetized, then the ION and ION-PD were injected intravenously with a 5 mg Fe/kg body weight ratio. The time interval between administration before the MR imaging was set to be 12 and 48h. ION and ION-PD's diagnostic efficacy was determined by acquiring T_2-weighted MR images using a fast spin echo sequence. The localized tumor site, in 12h and 48h post-injection, can be seen in the color map and MRI images in Fig. 5.

Aggregation of the ION-PD in the tumor was made plausible via binding to its specified receptor ligands of HER2. Therefore, the ION-PD exhibited protracted preservation in the tumor because of cellular endocytosis, decreasing the T_2 relaxation time. The signal intensity values in the ION-PD group at 12 h and 48 h post-injection demonstrate an overall reduction compared to other groups (Fig. 6). This incident can be elaborated by the

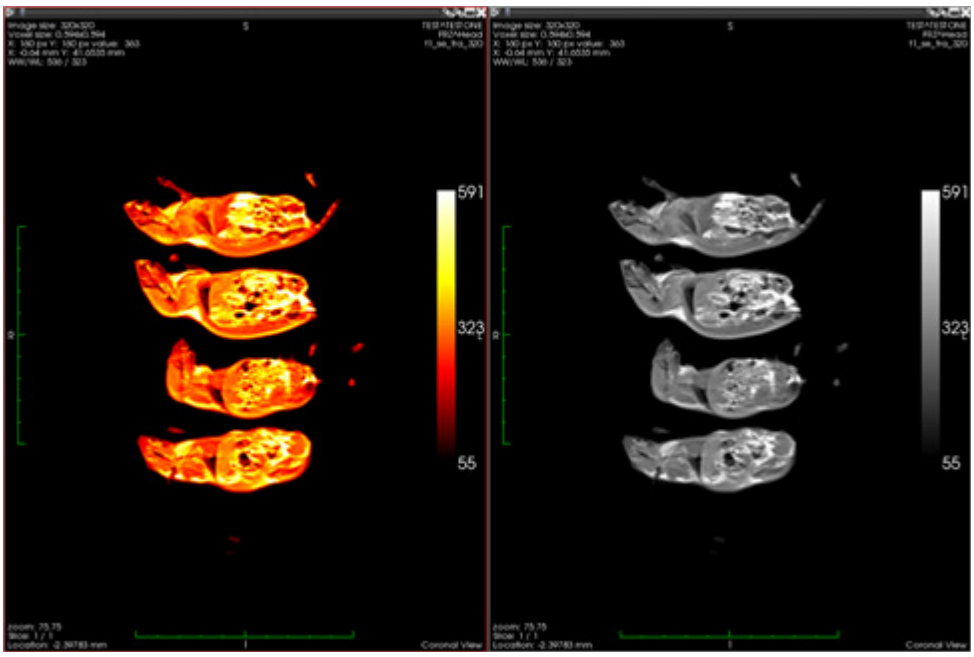

Fig. 5. Color map and MR images of ION and ION-PD samples. The first two upper mice were inject with ION-PD, and the red arrows are pointing out the aggregation sites of nanoprobes. The other two were injected with ION.

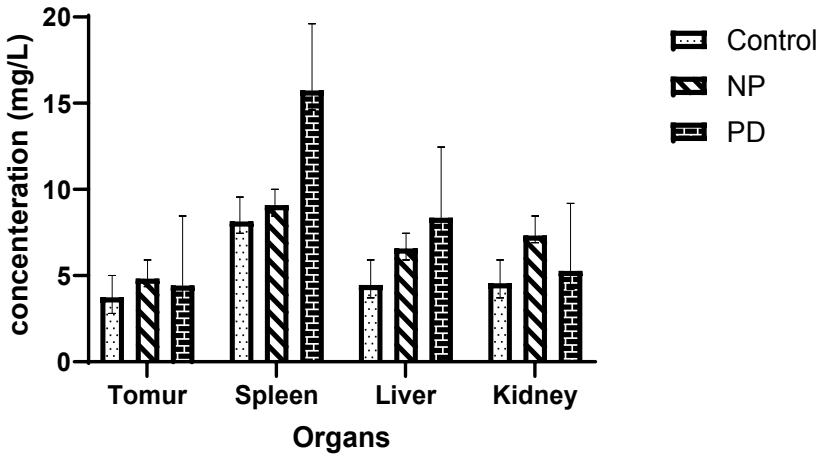

Fig 6. Comparison of Signal intensity for 12 h, and 48 h sample in the tumors.

binding role of Poly-dopamine as a synergistic motivator in uptaking ION-PD as an MR imaging nano contrast agent.

As depicted in the graph, the measured mean and standard deviation of signal intensity of breast tumors treated with ION-PD exhibit a larger reduction in 48 h compared to 12 h post-injection time (~5 percent decrease). Additionally, ION-PD decreased signal intensity by 8 percent in contrast to ION. Interestingly, the distribution pattern of ION-PD in the tumor was more uniform than ION due to its specialized targeting capacity, promoting cellular internalization. These results demonstrated that ION-PD nanoprobes potentially used T_2 contrast agents in breast cancer. The color-map images indicated that the cold spot regions corresponded to the lower signal intensity.

Fe concentration measurements

To assess the biodistribution of ION and characterize their targeting competency in the acid-digested critical organs of 12 h post-injection

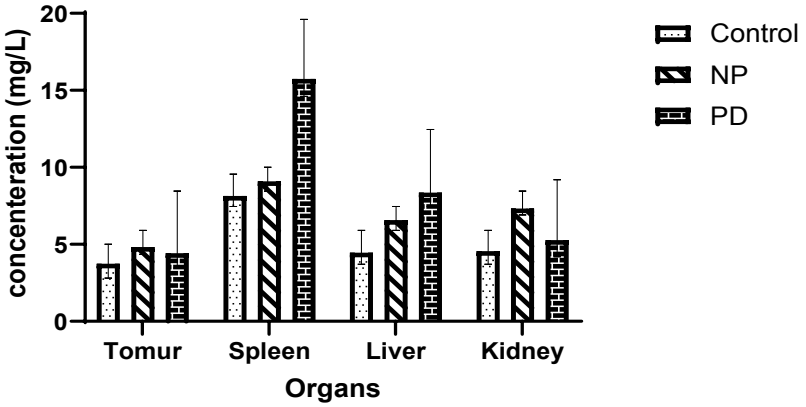

Fig. 7. Accumulation of ION and ION-PD in various organs of cancerous and control mice, 12 h post-injection.

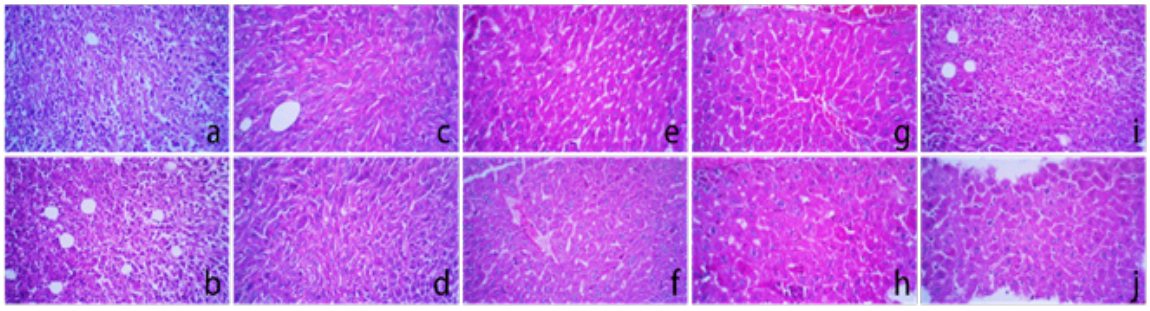

Fig. 8. Microscopic images of tumor and liver 12 h and 48 h post-injection. Hematoxylin and eosin stained ×40 magnification. a: control tumor, b: control liver, c: 48 h ION-PD liver, d: 48 h ION liver, e: 12 h ION-PD liver, f: 12 h ION liver, g: 12 h ION tumor, h: 12 h ION tumor, i: 48 h ION-PD tumor, j: 48 h ION tumor.

cancerous mice, an ICP-OES test was conducted. This quantitatively-analysis test measured the iron uptake in retrieved tissues of examined animals at 12 h after ION and ION-PD administration. The results indicated that the spleen met the highest concentration of ION and ION-PD with 15.74 and 9.093 mg/l, respectively (Fig. 7). Moreover, The ION and ION-PD distribution in the liver was 8.36 and 6.57 mg/l. Tumor and kidney uptake of ION-PD was higher than liver and spleen. ION-PD absorption for tumor and kidney was 4.82 and 7.322, while ION uptake was 4.421 and 5.268. A higher amount of ION in the liver than ION-PD was justifiable due to the clearing function of the liver. The significant amount of ION in the liver indicated that the liver is an organ via which the ION nanoparticle will be expelled from the body. These findings demonstrated using ION-PD as an MR imaging probe for particular breast cancer cells.

Histopathologic tissue study

The liver and tumor tissues were obtained 12 and 48 hours post-injection and immunostained using the hematoxylin and eosin methods. The image shows mild to severe levels of pathology in the liver and tumor cells (Fig. 8). Longer exposure of tissues to ION and ION-PD inflicts more severe damage.

Bacterial study

Isolation and identification of H.pylori

Among 110 biopsy samples collected from suspected patients, 60 samples (54.55%) were confirmed to be *H.pylori* based on their morphology observed under a microscope, colony shape, and positive results in catalase, oxidase, and urease biochemical tests.

Disc diffusion

The antibiotic susceptibility test for 60 *H.pylori* isolates was determined by the disk diffusion method for the antibiotic metronidazole. 20 isolates (33.33 %) of the examined strains were considered resistant due to having a growth inhibition zone of less than 16 mm. We used 12 of the 20 metronidazole-resistant *H.pylori* strains for further tests.

Minimum inhibitory determination

The minimum inhibitory concentration (MIC) results forION AND ION-PD and metronidazole

Table 1. MIC and MBC concentrations for Fe3O4 nanoparticles and Poly-dopamine coated-nanoprobes for 12 strains of H.pylori: broth microdilution method.

Sample No.	MIC of Metronidazole	MIC of Fe_3O_4	MBC of Fe_3O_4	MIC of Fe_3O_4@	MBC of Fe_3O_4@
1	16	4	8	16	16
2	32	8	16	16	32
3	64	4	4	32	32
4	16	16	32	64	128
5	16	4	16	16	32
6	16	4	32	32	64
7	128	16	32	64	128
8	64	8	8	32	128
9	16	4	8	16	32
10	32	32	32	64	128
11	128	8	64	32	128
12	16	8	16	16	32

MIC: minimum inhibitory concentration; MBC: minimum bactericidal concentration

ranged from 4 to 32 and 8 to 64 micrograms/ml and 16 to 128 micrograms/ml, respectively [Table 1].

After culturing the suspensions in the wells above the MICs on the Columbia blood agar medium, the results of the minimum bactericidal concentration of uncoated and polydopamine-coated nanoparticles were reported in the range of 4-64 and 16-128, respectively.

DISCUSSION

IONs bond through van der Waals interaction, requiring a shell to protect them from the environment, so various organic or mineral components coat their surface depending on their purpose. Since the coatings operate as parts of the ION surface exposed to various biological stimuli, they must be biocompatible with no related cytotoxicity. Several studies were carried out to utilize polymer-coated IONs with anti-cancer medications, and their results demonstrated that coated IONs were particularly suited for carrying and delivering therapeutics to target areas [33]. Materials having cell viability of more than 80 percent are considered biocompatible. Our study employed polydopamine as a coating agent for Fe_3O_4 nanoparticles. Coated IONs, such as Fe_3O_4@ PDA, demonstrated lower cytotoxicity for two reasons: 1. their coating was biocompatible; and 2. the coating reduced the adsorption sites for proteins, ions, and other environmental components [34].

ION's cytotoxicity is governed by its sizes, dimensions, chemical compositions, morphologies, surface structures, surface electric charges, density, and solubility [35]. IONs can induce oxidative stress (OS) via the Fenton reaction [$H_2O_2 + Fe_2 \rightarrow Fe_3 + HO^- + HO^{\bullet}$], which is considered the most prevalent source of reactive oxygen species (ROS) in biological systems. Increased oxidative stress and inflammatory products such as cytokines can cause mitochondrial collapse and DNA mutation, resulting in tissue necrosis. The mechanisms by which IONs generate ROS are still unknown, and it is hypothesized that disruption of the well-structured electronic configuration of the nano-sized material surface creates reactive electron donor or acceptor sites, forming superoxide radicals [36]. Additionally, uncoated IONs are cytotoxic, and their excessive dosages induce further tissue damage owing to OS [37]. Our findings demonstrated that the cytotoxicity of ION is dosage and time-dependent. The IC50 concentration, the least amount of ION-PD concentration required to mortify 50 percent of cancerous cells, was 128 μg/ml at 72 h incubation time. Thus, MCF-7 cell viability was more than 60 percent at all concentrations and incubation times (24, 48, and 72 h). Consequently, there was no indication of ION-PD toxicity, indicating the biocompatibility of the nanoprobe, with no significant changes at 48 and 72 h incubation, aligning with previous studies [38-40]. The maximum cytotoxicity is reported at 512 μg/ml, with viability of roughly 83 percent. MTT assay findings revealed that MCF-7 cells had the best survival rates at 128 μg/ml after 72 hours. At 24 h and 48 h, the ION-PD molecule is preferentially absorbed by the tumor. This strategy proved feasible in breast cancer diagnosis and can be used to achieve excellent T_2-W MR images at an early stage.

IONs are more magnetically susceptible than their oxidized counterparts; thus, they are better suited for MRI contrast agents. The mechanism in which Fe_3O_4 nanoparticles create contrast lies in the interaction they form with the surrounding tissues. The water molecules in the second sphere of this compound interact with the bulk water, affecting the rotational correlation time of the water molecules residing in the extracellular space. This phenomenon will cause a decrease in the T_1, and T_2 relaxation time of the surrounding water and thus faster recovery of hydrogen

spins in the spin-spin and spin-lattice networks, eventually leading to diminished signal intensity [41]. However, the extended impact of iron oxide nanoparticles on the spin-spin relaxation time is greater than the spin-lattice, which then makes it more applicable as a T_2 weighted contrast nano agent. The introduction of the poly-dopamine as a coating to the nanoparticles enhances the T_2-reduction effect even further, resulting in lesser signal intensity than ION and creating dark-appearing images. Based on the uptake concentration of ION-PD, it can be concurred that the spleen has the highest transverse relaxation rate (R2), followed by the liver, kidney and tumor. IONs present new possibilities for localized detection of breast cancer biomarkers, which can enhance breast cancer prognosis at an early stage [37]. The applicability of molecular imaging as a diagnostic modality for breast cancer can be determined by the access rate of ION to the tumor vascular system. However, one of the major obstacles in using MRI to diagnose breast cancer is determining how to increase the deposition of certain contrast agents on the breast tumor (specific antigen). This study showed that ION-PD could decrease the signal intensity of MR images and be considered a potential breast cancer contrast agent for T_2-W MR images.

The liver and tumor cells of the mice were immunostained using the H&E method and were observed by microscope. As Fig. 8 suggested, longer exposure of cells to ION and ION-PD caused more severe tissue damage. The nucleus integrity of the 48 h post-injection hepatocyte was lost, altering into the bi-nuclear cell. Cytoplasm became opaque, and overall cell volume was increased. Portal vein dilation was also observed, resulting from ION-induced vascular lesions. The damage inflicted by ION-PD to hepatocytes was significantly lower, including no vascular dilation, less cell volume, and granular appearance. 12 h post-injection, hepatocytes treated with ION-PD exhibited arranged nuclei with more lucent cytoplasm and less cell volume.

The size, charge, and delivery route of IONs can each affect their circulation period, and bio-aggregation outlines in the different organs. The spleen usually sequesters large nanoparticles (>200 nm) through mechanical clearance followed by phagocytosis, while smaller particles (<10 nm) are swiftly removed via extravasation and glomerular filtration. Upon *in vivo* ION administration, it was encountered by the macrophages of the Reticuloendothelial System (RES). The efficacy of RESION'ss clearance is based on the size and chemical composition of the IONs, which can influence macrophage activation and particle internalization. IONs can be internalized via phagocytosis, scavenger receptor-mediated endocytosis, fluid-phase endocytosis, and diffusion [42]. IONs promote the activation of phagocytotic, cytoskeletal, and cytokine-releasing functions of macrophages [43]. The high accumulation rate of ION-PD in the liver and spleen demonstrated that the nanoprobe is detoxified through the blood circulation system by the spleen and liver [44], indicating the biocompatibility of ION-PD. Typically, upon ION-PD's intracellular internalization via endocytosis, they became clustered within lysosomes and degraded into iron ions by a range of hydrolyzing enzymes at low pH according to endogenous iron metabolism pathways [45, 46]. However, ION aggregation in the kidney was higher than in the spleen and liver, which can be justified by the lesser filtration rate of coated nanoparticles in the glomerulus compared to non-coated nanoparticles. Similarly, the ION deposition in the tumor was higher than ION-PD due to angiogenesis and excessive vascularization of the tumor, which results in more ION deposition through afferent arteries. The previous study confirmed these results, in which radiolabeled IONs were utilized as a new type of nanoprobes and were thoroughly or partially filtered in mice, with minimal absorbance by the liver and other organs of the RES.

Moreover, the findings demonstrated considerable accumulation of ION-PD in the tumor at 12 hours post-injection. The mean ION content was notably higher at 12 h post-injection than in the control group. The mean iron content in the liver was substantially higher than in the other organs. The ION load in the breast cancer cell line (MCF-7) was %35 higher than the control group. This result indicated that the breast cancer-targeted nanoprobe (ION-PD) demonstrates its high affinity for indirectly diagnosing MCF-7 cells and anti-HER2 antibodies. Studies are underway to produce nanoparticles for cancer treatment utilizing numerous physical and chemical techniques as an alternative and integrated treatment technology [11].

In this experiment, we tried to evaluate the toxicity of ION and ION-PD on both eukaryotic (MCF-7 cancerous cell line) and prokaryotic (*H.pylori*) cells. The iron oxide nanoparticles had pronounced antibacterial effects on *H.pylori*; however, the polydopamine coating substantially lowered its toxicity. The MBC and MIC had no toxic effects on cancerous cell lines. The results obtained in our study align with previous studies, which reported MIC values ranging from 4 to 32 [47, 48]. However, it is important to note that our antibiotic sensitivity test was conducted on metronidazole-resistant strains, necessitating higher starting concentrations for MIC determination in our

research. This could be attributed to the activity of reactive oxygen species resulting from the absorption of metal ions through the cell membrane, followed by direct interaction with functional groups of proteins and nucleic acids, such as mercapto (-SH), amino (-NH), and carboxyl (-COOH). Additionally, nanoparticles' type, size, and dispersion are crucial in their impact on cellular efficacy (14).

CONCLUSION

The Fe_3O_4@Poly-dopamine nanoprobe was evaluated in vivo and ex vivo to detect the human epidermal growth factor receptor overexpressed in MCF-7 breast cancer cells. In breast cancer tumor-induced mice, the ION-PD considerably reduced signal intensity. Overall, the Fe_3O_4@Poly-dopamine has the potential to be implemented as an MR imaging nanoprobe for the identification of breast cancer (MCF-7) cells. In addition, the effects of ION-PD to inhibit the growth of *H.pylori* are notable.

AUTHOR CONTRIBUTIONS

Conceptualization, D.S.-G., and M.Gh.; Methodology, D.S.-G., M.Gh., F.H.B., A.S, G.-R.A, Aand M.R.S.; Software, M.Gh.; Validation, D.S.-G., and M.Gh, T.M, G.-R.A.; Formal Analysis, M.Gh., and D.S.-G.; Investigation, D.S.-G., and M.Gh.; Resources, D.S.-G., and M.Gh., and F.H.B.; Data Curation, M.Gh.; Writing—Original Draft Preparation, M.Gh, A.S.; Writing-Review and Editing, M.Gh., and D.S.-G.; Visualization, D.S.-G.; Supervision, M.R.S., and D.S.-G.; Project Administration, M.R.S, and D.S.-G.; Funding Acquisition, D.S.-G., and M.R.S. All authors have read and agreed to the published version of the manuscript.

ACKNOWLEDGMENT

This work was financially supported (Grant numbers 3400132, and 1400367) by Isfahan University of Medical Sciences, Isfahan, Iran.

ETHICAL CONSIDERATIONS

The Research Ethics Committee of Isfahan University of Medical Sciences, School of Medicine has confirmed the ethical code of IR.MUI.MED.REC.1400.236 and IR.ARI.MUI.REC.1400.063.

DATA AVAILABILITY STATEMENT

The experimental data used to support the findings of this study is available from the corresponding author upon request.

CONFLICTS OF INTEREST

The authors declare they have no conflict of interest.

REFERENCES

1. Al-Musawi S, Albukhaty S, Al-Karagoly H, Sulaiman GM, Jabir MS, Naderi-Manesh H. Dextran-coated superparamagnetic nanoparticles modified with folate for targeted drug delivery of camptothecin. Adv Nat Sci: Nanosci. 2020;11(4):045009.
2. Stanković A, Mihailović J, Mirković M, Radović M, Milanović Z, Ognjanović M, Janković D, Antić B, Mijović M, Vranješ-Đurić S, Prijović Ž. Aminosilanized flower-structured superparamagnetic iron oxide nanoparticles coupled to 131I-labeled CC49 antibody for combined radionuclide and hyperthermia therapy of cancer. Int J Pharm. 2020;587:119628.
3. Laurencin M, Cam N, Georgelin T, Clément O, Autret G, Siaugue JM, Ménager C. Human erythrocytes covered with magnetic core-shell nanoparticles for multimodal imaging. Adv Healthc Mater. 2013;2(9):1209-1212.
4. Albukhaty S, Al-Musawi S, Abdul Mahdi S, Sulaiman GM, Alwahibi MS, Dewir YH, Soliman DA, Rizwana H. Investigation of dextran-coated superparamagnetic nanoparticles for targeted vinblastine controlled release, delivery, apoptosis induction, and gene expression in pancreatic cancer cells. Molecules. 2020;25(20):4721.
5. Israel LL, Galstyan A, Holler E, Ljubimova JY. Magnetic iron oxide nanoparticles for imaging, targeting and treatment of primary and metastatic tumors of the brain. J Control Release. 2020;320:45-62.
6. Ankamwar B, Lai TC, Huang JH, Liu RS, Hsiao M, Chen CH, Hwu YK. Biocompatibility of Fe_3O_4 nanoparticles evaluated by in vitro cytotoxicity assays using normal, glia and breast cancer cells. Nanotechnology. 2010;21(7):075102.
7. Khaniabadi PM, Shahbazi-Gahrouei D, Jaafar MS, Majid AM, Khaniabadi BM, Shahbazi-Gahrouei S. Magnetic iron oxide nanoparticles as T_2 MR imaging contrast agent for detection of breast cancer (MCF-7) cell. Avicenna J Med Biotechnol. 2017;9(4):181.
8. Dheyab MA, Aziz AA, Khaniabadi PM, Jameel MS. Potential of a sonochemical approach to generate MRI-PPT theranostic agents for breast cancer. Photodiagnosis Photodyn Ther. 2021;33:102177.
9. Deda DK, Cardoso RM, Kawassaki RK, de Oliveira AR, Toma SH, Baptista MS, Araki K. Cytotoxicity of methotrexate conjugated to glycerol phosphate modified superparamagnetic iron oxide nanoparticles. J Nanosci Nanotechnol. 2021;21(3):1451-1461.
10. Beigi FH, Jazi SS, Shahbazi-Gahrouei D, Khaniabadi PM, Hafezi H, Monajemi R, Amiri GR. Iron oxide nanoparticles coated with polydopamine as a potential nano-photothermal agent for treatment of melanoma cancer: an in vivo study. Lasers Med Sci, 2022. 37(9):3413-3421.
11. Palanisamy S, Wang YM. Superparamagnetic iron oxide nanoparticulate system: synthesis, targeting, drug delivery and therapy in cancer. Dalton Trans.

2019;48(26):9490-9515.
12. Wang C, Wang Y, Xiao W, Chen X, Li R, Shen Z, Lu F. Carboxylated superparamagnetic Fe_3O_4 nanoparticles modified with 3-amino propanol and their application in magnetic resonance tumor imaging. BMC Cancer. 2023;23(1):54.
13. Liang M, Zhou W, Zhang H, Zheng J, Lin J, An L, Yang S. Tumor microenvironment responsive T 1–T 2 dual-mode contrast agent Fe_3O_4@ ZIF-8-Zn–Mn NPs for in vivo magnetic resonance imaging. J Mater Chem B. 2023;11(19):4203-4210.
14. Liu D, Li J, Wang C, An L, Lin J, Tian Q, Yang S. Ultrasmall Fe@ Fe3O4 nanoparticles as T_1–T_2 dual-mode MRI contrast agents for targeted tumor imaging. Nanomedicine. 2021;32:102335.
15. Liu X, Cao J, Li H, Li J, Jin Q, Ren K, Ji J. Mussel-inspired polydopamine: a biocompatible and ultrastable coating for nanoparticles in vivo. ACS Nano. 2013;7(10):9384-9395.
16. Gu X, Zhang Y, Sun H, Song X, Fu C, Dong P. Mussel-Inspired Polydopamine Coated Iron Oxide Nanoparticles for Biomedical Application. J Nanomater. 2015;2015(1):154592.
17. Liao N, Wu M, Pan F, Lin J, Li Z, Zhang D, Wang Y, Zheng Y, Peng J, Liu X, Liu J. Poly (dopamine) coated superparamagnetic iron oxide nanocluster for noninvasive labeling, tracking and targeted delivery of adipose tissue-derived stem cells. Sci Rep. 2016;6(1):18746.
18. Zhang T, Li Y, Hong W, Chen Z, Peng P, Yuan S, Qu J, Xiao M, Xu L. Glucose oxidase and polydopamine functionalized iron oxide nanoparticles: Combination of the photothermal effect and reactive oxygen species generation for dual-modality selective cancer therapy. J Mater Chem B. 2019;7(13):2190-2200.
19. Li S, Cao M, Song L, Qi P, Chen C, Wang X, Li N, Peng J, Wu D, Hu G, Zhao J. The contribution of toll-like receptor 2 on Helicobacter pylori activation of the nuclear factor-kappa B signaling pathway in gastric epithelial cells. Microb Pathog. 2016;98:63-68.
20. Poonyam P, Chotivitayatarakorn P, Vilaichone RK. High effective of 14-day high-dose PPI-bismuth-containing quadruple therapy with probiotics supplement for Helicobacter pylori eradication: a double blinded-randomized placebo-controlled study. Asian Pac J Cancer Prev. 2019;20(9):2859.
21. Cai Y, Wang C, Chen Z, Xu Z, Li H, Li W, Sun Y. Transporters HP0939, HP0497, and HP0471 participate in intrinsic multidrug resistance and biofilm formation in Helicobacter pylori by enhancing drug efflux. Helicobacter. 2020;25(4):e12715.
22. Hussein RA, Al-Ouqaili MT, Majeed YH. Detection of clarithromycin resistance and 23SrRNA point mutations in clinical isolates of Helicobacter pylori isolates: Phenotypic and molecular methods. Saudi J Biol Sci. 2022;29(1):513-520.
23. Fatahian S, Shahbazi D, Pouladian M, Yousefi MH, Amiri GhR SZ, Jahanbakhsh H. Preparation and magnetic properties investigation of Fe_3O_4 nanoparticles 99mTc labeled and Fe_3O_4 nanoparticles DMSA coated. Dig J Nanomater Bios. 2011;6(3):1161-1165.
24. Beigi, F.H., et al., Assessment of ploy dopamine coated Fe_3O_4 nanoparticles for melanoma (B16-F10 and A-375) cells detection. Anti-Cancer Agents in Medicinal Chemistry (Formerly Current Medicinal Chemistry-Anti-Cancer Agents), 2020. 20(16): 1918-1926.
25. Bahjat HH, Ismail RA, Sulaiman GM. Photodetection properties of populated Fe_3O_4@ TiO2 core–shell/Si heterojunction prepared by laser ablation in water. Appl Phys A. 2022;128(1):8.
26. Ahmadian S, Barar J, Saei AA, Fakhree MA, Omidi Y. Cellular toxicity of nanogenomedicine in MCF-7 cell line: MTT assay. J Vis Exp. 2009(26):e1191.
27. Clark JD, Gebhart GF, Gonder JC, Keeling ME, Kohn DF. The 1996 guide for the care and use of laboratory animals. Ilar j, 1997; 38(1): 41-48.
28. Shahbazi-Gahrouei D, Abdi N, Shahbazi-Gahrouei S, Hejazi SH, Salehnia Z. In vivo study of anti-epidermal growth factor receptor antibody-based iron oxide nanoparticles (anti-EGFR-SPIONs) as a novel MR imaging contrast agent for lung cancer (LLC1) cells detection. IET nanobiotechnology. 2020;14(5):369-374.
29. Mirzaei N, Poursina F, Faghri J, Talebi M, Khataminezhad MR, Hasanzadeh A, Safaei HG. Prevalence of resistance of Helicobacter pylori strains to selected antibiotics in Isfahan, Iran. Jundishapur J Microbiol. 2013;6(5).
30. Hussein RA, Al-Ouqaili MT, Majeed YH. Association between alcohol consumption, cigarette smoking, and Helicobacter pylori infection in Iraqi patients submitted to gastrointestinal endoscopy. J Emerg Med Trauma Acute Care. 2022;2022(6):12.
31. Rezaei S, Abadi AT, Mobarez AM. Metronidazole-resistant Helicobacter pylori isolates without rdxA mutations obtained from Iranian dyspeptic patients. New Microb New Infec. 2020;34:100636.
32. Hossein-Beigi F, Fatahian S, Shahbazi-Gahrouei D. In-vitro toxicity assessment of polydopamine-coated and uncoated Fe_3O_4 nanoparticles in cell line B16-F10 (Melanoma Cell). J Isfahan Med Sch. 2019;37(533):762-767.
33. Alexis F, Pridgen E, Molnar LK, Farokhzad OC. Factors affecting the clearance and biodistribution of polymeric nanoparticles. Mol Pharm. 2008 Aug 4;5(4):505-515.
34. Eivazi M, Khaniabadi PM, Hejazi SH, Shahbazi-Gahrouei D. Porphyrin–iron oxide nanoparticle functionalized with trastuzumab (ION–PP–TZ) potential MR imaging probe for breast cancer cells. Appl Phys A. 2022;128(6):509.
35. Ito A, Shinkai M, Honda H, Kobayashi T. Medical application of functionalized magnetic

nanoparticles. J Biosci Bioeng. 2005;100(1):1-1.
36. Nel A, Xia T, Madler L, Li N. Toxic potential of materials at the nanolevel. Science. 2006;311(5761):622-627.
37. Frantellizzi V, Conte M, Pontico M, Pani A, Pani R, De Vincentis G. New frontiers in molecular imaging with superparamagnetic iron oxide nanoparticles (SPIONs): efficacy, toxicity, and future applications. Nucl Med Mol Imaging. 2020;54:65-80.
38. Mustafa TA, Mohammed-Rasheed MA. Accumulation and cytotoxicity assessment of TAT-IONPs on cancerous mammalian cells. Anim Biotechnol. 2021;32(1):100-105.
39. Voss L, Hoché E, Stock V, Böhmert L, Braeuning A, Thünemann AF, Sieg H. Intestinal and hepatic effects of iron oxide nanoparticles. Arch Toxicol, 2021. 95(3): 895-905.
40. Miri A, Najafzadeh H, Darroudi M, Miri MJ, Kouhbanani MA, Sarani M. Iron oxide nanoparticles: biosynthesis, magnetic behavior, cytotoxic effect. ChemistryOpen. 2021;10(3):327-333.
41. Jeon M, Halbert MV, Stephen ZR, Zhang M. Iron oxide nanoparticles as T_1 contrast agents for magnetic resonance imaging: fundamentals, challenges, applications, and prospectives. Adv Mater. 2021;33(23): e1906539.
42. Unfried K, Albrecht C, Klotz LO, Von Mikecz A, Grether-Beck S, Schins RP. Cellular responses to nanoparticles: target structures and mechanisms. Nanotoxicol. 2007;1(1):52-71.
43. Dobrovolskaia MA, McNeil SE. Immunological properties of engineered nanomaterials. Nano Sci Technol J. 2010: 278.
44. Park JH, Von Maltzahn G, Zhang L, Schwartz MP, Ruoslahti E, Bhatia SN, Sailor MJ. Magnetic iron oxide nanoworms for tumor targeting and imaging. Adv Mater. 2008;20(9):1630-1635.
45. Gupta AK, Naregalkar RR, Vaidya VD, Gupta M. Recent advances on surface engineering of magnetic iron oxide nanoparticles and their biomedical applications. Nanomed. 2007;2(1):23-39.
46. Al-Ouqaili MT. Depending on HPLC and PCR, detection of aflatoxin B1 extracted from Aspergillus flavus strains and itâ€™ s cytotoxic effect on AFB treated-hematopoietic stem cells obtained from human umbilical cord. Asian J Pharm. 2018;12(3).
47. Kim JM, Kim JS, Kim N, Kim SG, Jung HC, Song IS. Comparison of primary and secondary antimicrobial minimum inhibitory concentrations for Helicobacter pylori isolated from Korean patients. Int J Antimicrob Agents. 2006;28(1):6-13.
48. Kato S, Fujimura S, Udagawa H, Shimizu T, Maisawa S, Ozawa K, Iinuma K. Antibiotic resistance of Helicobacter pylori strains in Japanese children. J Clin Microbiol. 2002;40(2):649-653.